Competition Between Water-Water Hydrogen bonds and Water-π Bonds in Pyrene-Water Cluster Anions

Heinrich Salzmann,[a,b] *Anne P. Rasmussen,*[a,c] *Joel D. Eaves,*[b] *J. Mathias Weber*[a,b] *

[1] JILA, University of Colorado, Boulder, CO 80309-0440, USA

[2] Department of Chemistry, University of Colorado, Boulder, CO 80309-0215, USA

[3] Department of Physics and Astronomy, Aarhus University, 8000 Aarhus, Denmark

KEYWORDS.

Pyrene; polyaromatic hydrocarbons; water clusters; vibrational spectroscopy; hydrogen bonding

TOC Graphic

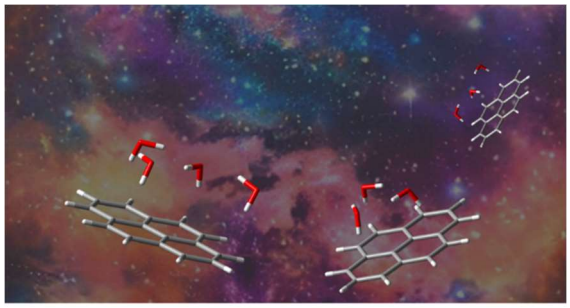

ABSTRACT

We present infrared spectra and density functional theory calculations of hydrated pyrene anion clusters with up to four water molecules. The experimental spectra were acquired using infrared Ar messenger photodissociation spectroscopy. Water molecules form clusters on the surface of the pyrene, forming hydrogen bonds with the π-system. The structures of the water clusters and their interaction with the π system are encoded in the OH stretching vibrational modes. We find that the interactions between water molecules are stronger than between water molecules and the π-system. While all clusters show multiple conformers, three- and four-membered rings are the lowest energy structures in the larger hydrates.

I. Introduction

Interactions of water with polyaromatic forms of carbon are of interest in a variety of chemical contexts. Polyaromatic hydrocarbons (PAHs) act as pollutants in brown carbon haze[1-3] as well as other atmospheric aerosols,[4-7] and they are thought to occur in astrochemical dust and ices.[8-13] Moreover, the use of graphene in future applications in aqueous environments requires a detailed understanding of the interaction of water with π aromatic systems.[14-15]

Studying such interactions in condensed phase aqueous environments faces various problems. The interactions of water molecules with aromatic systems is encoded mainly in the infrared (IR) OH stretching vibrations of interfacial water, whose signatures are buried in the broad spectroscopic response of bulk water. Spectroscopic investigations of bulk aqueous solutions of PAHs suffer from their low solubility, and observation of clean spectroscopic signatures for water interactions with crystalline PAH surfaces is plagued by surface heterogeneity. Experiments on single layer graphene deposited on substrates are hindered by the wetting transparency of graphene,[16] and the preparation of free-standing single layer graphene is very challenging due to the formation of defects, the adsorption of hydrocarbons, and the fragility of extended single layer graphene sheets. The theoretical treatment of this problem has challenges of its own. Bulk aqueous systems are too large to be treated by high level quantum chemical methods, and computationally affordable descriptions of bulk aqueous systems rely on sufficiently parametrization of the water-water and water-carbon interactions, which are difficult to benchmark, since experimental results are hard to obtain. In particular, the subtle balance between collective phenomena (e.g., polarization of the liquid) and molecular-level effects (e.g., hydrogen bonding) complicates the systematic improvement of theoretical models for water-PAH interactions.

IR spectroscopy of hydrated clusters, combined with mass spectrometric preparation and detection, has been a molecularly specific and effective approach[17-24] to circumvent many of the intrinsic problems in the condensed phase. In particular, the use of mass-selected cluster ions as spectroscopic targets removes uncertainties due to speciation and heterogeneity of condensed phase environments, as both the nature of the PAH and the number of water molecules present are under rigorous experimental control. Computationally, this approach affords treatment with quantum chemical methods, and it allows to explore molecular level details of the structure and dynamics governed by intramolecular interactions between water molecules and solute ions, including anharmonic[25-28] and quantum nuclear[25, 29-30] effects. This approach allows to focus on molecular-level details of water-PAH and water-water interactions, since the small size of the clusters minimize collective effects, such as density and polarization fluctuation of the bulk.

The interaction between PAHs and water depends strongly on the charge state of the PAH. Water molecules bind to cationic PAHs (both radical ions and protonated species) through the interaction of the lone pairs on the O atoms with the CH groups on the periphery of the PAH.[31-34] These cluster systems inform on the interaction between water molecules and H-terminated edges along the periphery of the π-conjugated systems. In contrast, water makes primary contacts directly with the π system of PAHs for neutral[35-39] and anionic[40-44] clusters. In all cases, water molecules form hydrogen bonds (H-bonds) with each other, generating water clusters that bind to the PAH frame. In simple terms, the molecular structure and spectrum of the hydrated cluster results from the competition between water-water H-bonds and water-π bonds. For small water-PAH clusters, the relative strength of water-water H-bonds compared to water-π bonds are difficult to measure directly, but assignment of the IR features to the normal modes of the water network together with

the analysis of the frequencies and the amplitude contributions of each OH oscillator allows such an evaluation.[43]

Most of the available data on hydrated anionic PAHs describes hydrated naphthalene[40-43] (Np) anions. Experiments yielding structural information on larger hydrated PAHs address the question on how the size and shape of the PAH, which provides a structural template for the water network, influences the size and shape of the water subcluster. Small PAHs, such as Np, can induce geometric frustration of the water network. Pyrene (Py, $C_{16}H_{10}$) is a prototypical, planar PAH with four fused six-membered aromatic rings, and we use it as a model for the interaction of water with a more extended aromatic π system than Np. Previous photoelectron spectroscopy work by Verlet and coworkers[44] showed how the electronic states of the anion are stabilized by hydration. In the present work, we study water-π interactions using IR messenger tagging spectroscopy of mass-selected hydrated pyrene radical anion clusters with up to four water molecules, $Py^{-}\cdot(H_2O)_n$ (n = 1 – 4). We compare the experimental spectra with calculated spectra from static, density functional theory (DFT).

II. Methods

A. Experimental

Cluster ions of the form $Py^{-}\cdot(H_2O)_n\cdot Ar_m$ were prepared in a supersonic entrainment source described previously.[43, 45-46] We entrained Py vapor from a copper oven (T = 400 ± 10 K) and water vapor (at room temperature) from a pulsed valve (General Valve Series 9) into a pulsed supersonic expansion of argon (Even Lavie valve, stagnation pressure 1.5 bar). An electron beam (800 eV kinetic energy) injected into the high-density region of the expansion created a plasma, where attachment of low-energy secondary electrons to molecules and clusters created negative

ions. These anions were accelerated perpendicular to the expansion in a home-built Wiley-McLaren time-of-flight mass spectrometer, where the target ions for a given experiment were mass-selected employing a pulsed mass gate.[47] In the present work, we focus on clusters $Py^-\cdot(H_2O)_n\cdot Ar_2$ (n = 0 – 4). The target ions were irradiated with the output of a pulsed, tunable OPO/OPA system (LaserVision, pulse duration 5 – 7 ns, bandwidth ca. 2 cm^{-1}, pulse energy ca. 5-10 mJ). Photon absorption by target ions $Py^-\cdot(H_2O)_n\cdot Ar_2$ resulted in fragmentation according to

$$Py^-\cdot(H_2O)_n\cdot Ar_2 + \hbar\omega \rightarrow Py^-\cdot(H_2O)_n + 2\ Ar$$

We used two Ar atoms as messenger tags throughout the present work to suppress background signals from loss of a single Ar atom by unimolecular decay. Fragment ions $Py^-\cdot(H_2O)_n$ were selectively monitored after using a two-stage reflectron as a second mass spectrometry step, and they were detected on a dual microchannel plate.

The fragment ion intensity was monitored as a function of the IR wavenumber, and was normalized by the photon fluence to generate IR photodissociation spectra. Several spectra taken on different days were averaged for each target ion species to ensure reproducibility and the improve signal-to-noise ratio. The spectra were calibrated using a photoacoustic spectrum of water vapor[48] acquired in a home-built, 3D printed photoacoustic spectrometer.

B. Computational

Geometry optimized structures of possible conformers were calculated using DFT,[49] utilizing ωB97DX functional[50] and def2-TZVPP basis sets[51] for all atoms as implemented in Gaussian 16.[52] We found the potential energy surface of Py^--water interactions to contain multiple, extended basins, with very low frequency vibrational modes. To improve the quality of the structures, "very-tight" convergence criteria (root-mean-square force 10^{-6} H/Å) and a "SuperFine" integration grid

were chosen. In cases of failed geometry optimization steps, a quadratic convergence (SCF = QC) was used. The harmonic calculations were scaled by 0.9431 to match the lowest energy OH stretching feature in the experimental pyrene dihydrate anion spectrum. Consistent with prior work which examined the accuracy of various charge assignment methods,[46] partial charges were determined using Merz-Singh-Kollman (electrostatic potential, ESP) method.[53-54]

III. Results and Discussion

A. Overview

Figure 1 shows the IR photodissociation spectra of $Py^{-}\cdot(H_2O)_n\cdot Ar_2$ (n = 0 – 4), recorded by monitoring the loss of both Ar atoms. There are two regions of interest, the OH stretching region (ca. 3300 – 3750 cm^{-1}) and the CH stretching region (2900 – 3100 cm^{-1}). The OH stretching region shows spectra of increasing complexity with growing level of hydration, while the CH stretching region only exhibits small changes. We will discuss the two different regions in detail in the following sections.

Different from Np and phenanthrene, Py is sufficiently large to have a robust, positive adiabatic electron affinity (AEA) of 0.406 ± 0.010 eV.[44] As a result, the CH stretching transitions shown in Figure 1 are below the threshold for photodetachment, even for n = 0. Since the addition of each water molecule adds ca. 0.24 eV to the AEA,[44] all vibrational excitations in the fundamental OH stretching region of $Py^{-}\cdot(H_2O)_n$ clusters are also below the threshold for photodetachment. We therefore exclude processes involving the detachment continuum from our discussion.

The presence of two Ar atoms in the target clusters not only allows the use of messenger predissociation spectroscopy, but also ensures that the clusters are cold. Assuming that the species in the cluster ion beam are formed in an evaporative ensemble,[55] the energy in each cluster is of

the order of the binding energy of the last particle that was evaporated during cluster formation. This results in cluster temperature analogues estimated to be in the range of 50-100 K.

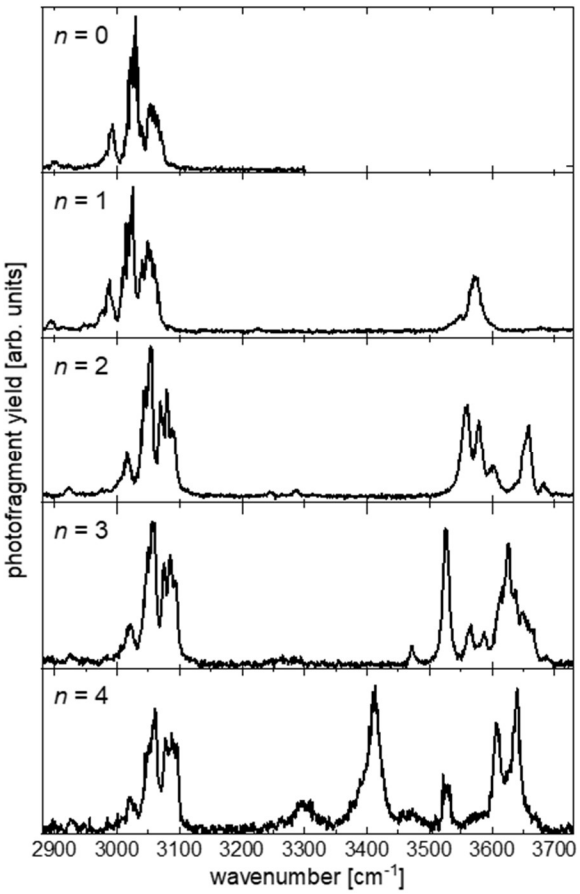

Figure 1. Infrared photodissociation action spectra of $Py^{-}\cdot(H_2O)_n\cdot Ar_2$ with n indicated in each panel. Data for n = 1 have been taken from ref. [46].

B. OH Stretching Region

1. Monohydrate (n = 1)

The spectrum of the Py monohydrate anion has been described in detail in recent work,[46] and we will only provide a brief discussion here. The OH stretching region of the photodissociation spectrum $Py^-\cdot H_2O\cdot Ar_2$ is reproduced in Figure 2. It is dominated by the signature of the symmetric OH stretching mode (ω_s) of the water molecule at 3573 cm^{-1}, while the feature encoding the antisymmetric stretching mode (ω_a) at ca. 3679 cm^{-1} is weak. Another very weak peak at 3225 cm^{-1} (see Figure 1) is in a region of the spectrum where the first overtone of the water bending mode is found in the spectra of other singly hydrated anion clusters.[56] The overtone borrows intensity through a Fermi resonance with the symmetric OH stretching mode, but in the present case, the substantial difference between the bending overtone and ω_s leads to a very low intensity.

Static DFT calculations at the level reported here return two low-energy, shallow minima in the potential energy surface, which correspond to two different configurations of the water molecule with respect to the Py^- anion (see Figure 3). Their calculated energies are within 2 meV, making the two structures isoenergetic. In both, the water molecule is engaged in a H-bond to the π system of the Py^- anion through one of its OH groups, while the second OH group is more weakly interacting with the PAH, but is not considered free. The signature of ω_a is observed at significantly lower wavenumbers than what is typical for a free OH (ca. 3710 cm^{-1}),[19, 56] corroborating this characterization. Their calculated spectra are both compatible with the experimental spectrum, but it is unclear which of these structures exist or are populated. The experimental spectrum merely allows the qualitative identification of the water-Py interactions, not the position of the water molecule on the Py^- frame.

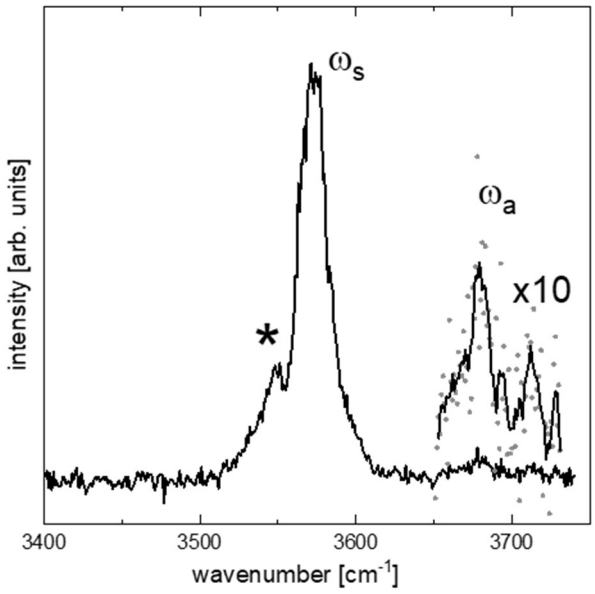

Figure 2. Infrared photodissociation spectrum of $Py^{-}\cdot H_2O\cdot Ar_2$ (data taken from ref. [46]). The labels ω_s and ω_a are attached to the features of the symmetric and antisymmetric OH stretching vibrations of the water molecule, respectively. The region of the latter is magnified by a factor of 10 as an inset, with grey dots being data points, and the line a 5-point gliding average to guide the eye.

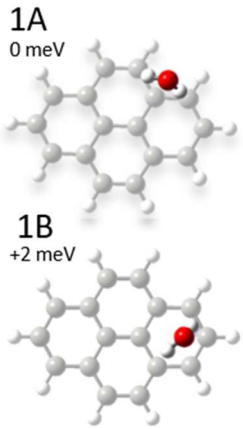

Figure 3. Low-lying minimum energy structures of $Py^{-}\cdot H_2O$ (structures taken from ref. [46]). The calculated energy of structure 1A is lower by 2 meV than for structure 1B. Color scheme: C = grey, H = white, O = red. The Py^{-} frame has been de-emphasized to more clearly show the water positions.

The origin of the shoulder on the low energy side of ω_s is unclear. It could be caused by two thermally populated, spectroscopically distinguishable structures whose individual ω_s signatures are split by 28 cm^{-1}. An alternative explanation involves coupling between ω_s and a low-frequency water rocking mode with a calculated frequency near 30 cm^{-1}, giving rise to a Franck-Condon-like progression. Finally, dynamic effects could lead to the observed line shape of the ω_s signature. Both classical and Born-Oppenheimer molecular dynamics on PAH water complexes[39, 46] show that the water molecule will explore a large part of the very shallow potential energy landscape, and the large linewidth of ω_s can in fact be attributed to dynamical broadening through spectral diffusion.[46] Unfortunately, none of these approaches explains the low energy shoulder of ω_s sufficiently well in the present calculations.[46] The origin of the substructure of the ω_s signature remains therefore an open question, highlighting the difficulty to correctly compute the potential energy surface of this seemingly simple complex.[46]

2. Dihydrate (n = 2)

Figure 4 presents the IR photodissociation spectrum of $Py^-\cdot(H_2O)_2\cdot Ar_2$ in the OH stretching region. The overall spectral envelope has some similarities to that of $Np\cdot(H_2O)_2$,[43] but the presence of five distinct spectral features for a species with four OH groups suggests the presence of more than one conformer. The lowest energy geometries for the dihydrate are characterized by a water dimer interacting with the Py^- anion (see Figure 5). In the two lowest energy structures, one water molecule is located above one of the central rings of Py^-, while the other is located over one of the outer rings. The main difference between the two structures is that the H-bond connecting the two water molecules is pointing in the opposite direction. The donor water molecule in the lowest

energy structure (2A) is located over an outer ring, while the acceptor molecule is over one of the inner rings. In structure 2B, calculated just 16 meV higher in energy, the role of the two water molecules is reversed. An additional structure (2C) with the water dimer mostly straddling an outer carbon ring is found 38 meV above the lowest energy structure. We note that the structure of the water subcluster in each of these geometries is very similar, and while the calculated relative energies imply a specific energetic ordering, the accuracy of the calculations and the small energy differences do not allow an unambiguous determination of the minimum energy structure. In each case, three OH groups interact with the π-system of the Py^- ion, and one OH group of the acceptor water molecule is interacting more strongly with the π-system of the Py^- ion than the other. As a result, the spectra of all three structures are very similar as well. Of course, the D_{2h} symmetry of the Py^- nuclear frame implies that there are eight equivalent, indistinguishable minima on the potential energy surface for each of the two structural conformers shown in Figure 5, four on each face of the PAH. While there are structures consisting of two independent water molecules (see Supporting Information), either on the same face of the PAH or on opposite faces, these structures are significantly higher in energy (> 100 meV above structure 2A), and their spectra are not consistent with the experimental spectrum.

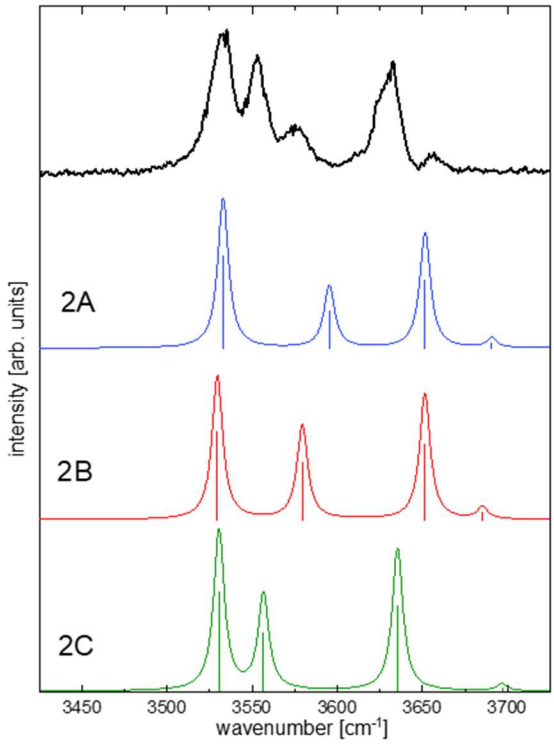

Figure 4. Infrared photodissociation spectrum of $Py^{-}\cdot(H_2O)_2\cdot Ar_2$ (top trace) in comparison with calculated IR spectra of the two lowest energy conformers (conformer label given for each curve, see Figure 5). The vertical sticks denote calculated frequency positions and intensities, the full lines show simulated spectra with 8 cm^{-1} full width at half-maximum (FWHM).

If only a single conformer were to give rise to the observed experimental spectrum, we would expect only four OH stretching features peaks. The calculated energy differences are sufficiently small to assume that structures 2A and 2B are isoenergetic for all practical purposes, and the energy of structure 2C is so close to the other two that we assume it to be thermally populated, even at the low temperatures of the ions in the present experiment. Since we observe five features with unresolved substructures, we assume that all three low lying structures are populated in the experiment.

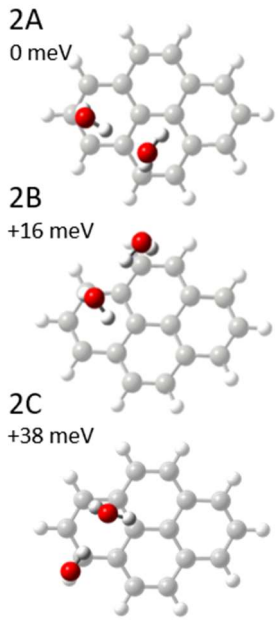

Figure 5. Low-lying minimum energy structures of $Py^{-}\cdot(H_2O)_2$, with relative energies given below each structure. Color scheme: C = grey, H = white, O = red. The Py^{-} frame has been de-emphasized to more clearly show the water positions.

The amplitude pattern of each vibrational mode is interesting, since it encodes which OH groups are characteristic of the mode, and together with the frequency of the mode, this information can allow us to draw conclusions about the interaction strength in a given H-bond. In the dihydrate spectrum, the lowest frequency mode is due to the in-phase linear combination of the two local symmetric OH stretching motions, and the OH group engaged in the water-water H-bond has the largest amplitude for all geometries considered here (2A–2C). This implies that the water-water interaction is the strongest intermolecular interaction in this cluster, which is at first glance surprising, given that the ion-water interaction is generally stronger than water-water interaction in many small hydrated anion clusters.[19, 57] However, a similar hierarchy of interaction strength has previously been observed in analogous $Np^{-}\cdot(H_2O)_n$ clusters.[43] The next higher energy mode is

associated with the out-of-phase linear combination, and is carried predominantly by the H-bond acceptor molecule. For each geometry, the feature with the second highest intensity (and the second highest frequency) is the signature of a mode mostly associated with the antisymmetric stretching motion of the H-bond donor molecule, while the weakest and highest frequency feature is mainly due to the antisymmetric stretching motion of the acceptor molecule.

We assign the feature at 3530 cm^{-1} to the in-phase linear combination of the symmetric stretching motions of the two water molecules. The calculated frequency positions for the three conformers are very close together, and we assume that all three conformers contribute to this feature. Based on the sequence of the calculated bands and their relative intensities, we tentatively assign the feature at 3551 cm^{-1} to the out-of-phase linear combination of the symmetric stretching motions for structure 2C, while the peak at 3574 cm^{-1} is likely the signature of this mode for conformers 2A and 2 B. The peak at 3631 cm^{-1} and the unresolved shoulder on its lower frequency side are the lower frequency combinations of the antisymmetric stretching motions for the three conformers, and the weak peak at 3654 cm^{-1} contains the analogous higher frequency components.

A close look at the overview spectrum shown in Figure 1 reveals two weak peaks at 3217 cm^{-1} and at 3258 cm^{-1}. Similar to the monohydrate, these peaks are in the region of the water bending mode overtone, and we therefore assign the two peaks qualitatively to these overtones.

We found three structures that we characterize as belonging to conformer family 2A, which differ very slightly in their geometries (see Supporting Information). While none of them are predicted to have imaginary frequencies, their energies are within 8 meV of each other, and we assume that they merely represent the same shallow potential energy basin of the lowest energy conformer. All of them have very low lying vibrational modes (< 50 cm^{-1}), which represent changes in the orientation of the water-water H-bond above the PAH frame, and a sliding of the

water dimer along the direction of the water-water H-bond. While our structural search revealed only one geometry each for conformers 2B and 2C, they possess similar low energy vibrational modes. The exploration of these shallow basins on the potential energy surface very likely leads to a dynamic line broadening, which we attribute to the relatively large linewidth in the OH stretching region, similar to the monohydrate.[46]

3. Trihydrate (n = 3)

The IR photodissociation spectrum of $Py^-\cdot(H_2O)_3\cdot Ar_2$ in the OH stretching region is given in Figure 6. It shows a complex set of features, which are clearly too numerous to be caused by a single conformer. The three lowest energy structures of $Py^-\cdot(H_2O)_3$ are shown in Figure 7. Very different from the mono- and dihydrate, the energy difference between the lowest energy conformers is significant, with a three-membered, homodromic ring (3A) clearly emerging as the lowest energy conformer, highlighting the cooperativity effects of partial delocalization of the proton wave functions in a H-bonded ring.[25] The next higher structure, a bent chain geometry (3B), is higher by 117 meV, and a second chain-like conformer (3C) is found at 160 meV above the ring structure.

The overall spectral pattern of the trihydrate spectrum is dominated by two prominent peaks at 3496 cm^{-1} and 3596 cm^{-1}. These two peaks are qualitatively consistent with the dominant features in the calculated spectrum of the ring conformer (3A). We attribute the weaker features to either of the chain conformers 3B and 3C, but will refrain from a more detailed assignment, given that the agreement between computed and experimental spectra is only qualitative. The energy difference between the ring and chain conformers cannot be bridged by thermal population of conformers, so we assume that different higher energy conformers are kinetically trapped during the cluster formation process in the supersonic expansion.

The intense lower frequency feature of the ring conformer contains two unresolved transitions, which are two linear combinations of OH stretching modes that are largely carried by OH groups involved in water-water H-bonds (labeled w in the experimental spectrum), but have different relative phases for the motion of each OH oscillator. A third, all in-phase linear combination (labeled w_{ip}) is predicted to be lower in intensity and ca. 65 cm^{-1} lower than the more prominent feature. While the amplitudes in the OH groups involved in H-bonding to the π system are much smaller than those of the H-bonded OH groups, we can still identify the character of the modes in the lower frequency transitions as local symmetric OH stretching modes.

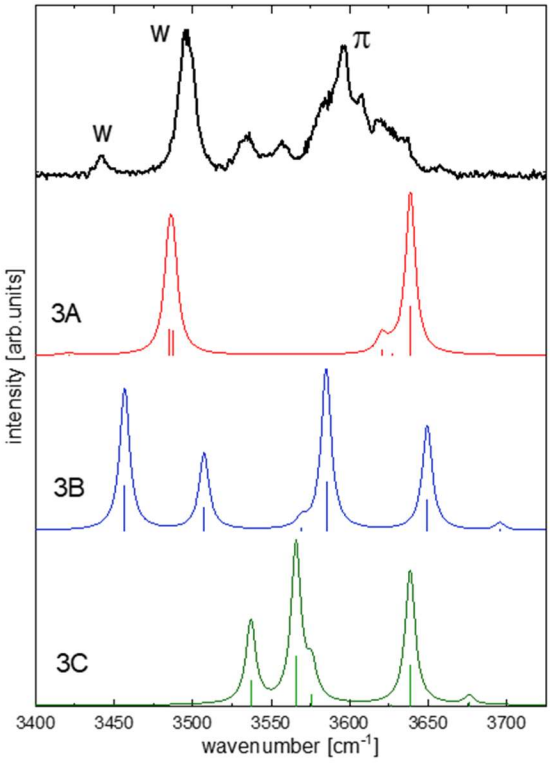

Figure 6. Infrared photodissociation spectrum of $Py^{-}\cdot(H_2O)_3\cdot Ar_2$ (top trace) in comparison with calculated IR spectra of the three lowest energy conformers (conformer label given for each curve, see Figure 7). The vertical sticks denote calculated frequency positions and intensities, the full lines show simulated spectra with 8 cm^{-1} full width at half-maximum (FWHM).

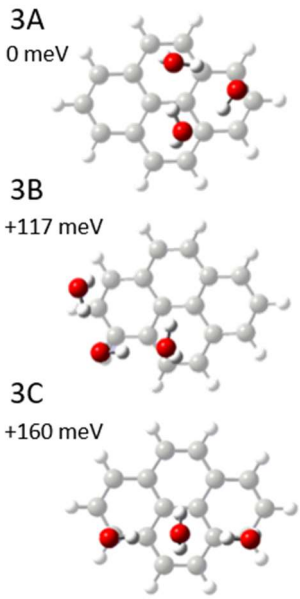

Figure 7. Low-lying minimum energy structures of $Py^{-}\cdot(H_2O)_3$, with relative energies given below each structure (see Supporting Information for additional structures). Color scheme: C = grey, H = white, O = red. The Py^{-} frame has been de-emphasized to more clearly show the water positions.

In analogy to the set of lower energy transitions, the higher energy feature at 3596 cm^{-1} (labeled π) contains three unresolved vibrational modes that are characterized mainly by the motion of the OH groups interacting with the π system of the Py^{-} anion. The most intense of these modes corresponds to the all-in-phase linear combination of these oscillators, which have the local character of antisymmetric OH stretching modes. The energetic ordering of the two groups of ring modes make a very clear case for the notion we made above that water-water interaction is significantly stronger than water-π interactions, despite the fact that the π system is charged.

The water bending mode overtone region of the trihydrate is characterized by a broad feature around 3233 cm^{-1}. It has an overall greater relative intensity, which is consistent with the fact that the symmetric stretching modes are now closer to the bending overtone frequencies, allowing more intensity borrowing.

4. Tetrahydrate (n = 4)

The IR photodissociation spectrum of $Py^{-}\cdot(H_2O)_4\cdot Ar_2$ (Figure 8) exhibits three strong peaks at 3382 cm^{-1}, 3577 cm^{-1}, and 3609 cm^{-1}, as well as a few weaker features. The basic structural motif of the calculated low energy structures (Figure 9) is the formation of rings, where a homodromic, four-membered ring represents the lowest energy structure (4A). Next higher in energy is a conformer with a three-membered ring similar to the trihydrate conformer 3A, with one additional water molecule that donates one H-bond to one of the water molecules in the ring, and one to the π system (4B). Again slightly higher in energy is a family of structures consisting of a three-membered ring with an additional water molecule forming two H-bonds to two water molecules in the ring (4C). There are three different possible positions, two in which the additional water molecule is over the Py edge, and one where it is over a carbon ring (see Supporting Information). The calculated energies of these structures are all within 10 meV of each other, and their calculated spectra are very similar. Next higher in energy is a class of geometries with a three-membered ring on one face of the PAH frame, and a single water molecule on the other, representing a combination of structure 3A with a monohydrate (Supporting Information). The structures based on three-membered rings are more than 250 meV higher in energy than the four-membered ring. Other structures, such as a prism or a pair of water dimers on different faces of the Py frame are significantly higher in energy (Supporting Information).

The calculated spectrum of the four-membered ring conformer (4A) qualitatively captures the three intense features of the spectrum. The lower energy range with a strong peak at 3382 cm^{-1} (labeled w) contains linear combinations of the symmetric stretching motions of the water molecules, although the amplitude patterns show motion mainly in the OH groups engaged in

water-water H-bonds. The patterns of motion of the four linear combinations in this group are given in Supporting Information. Only two of the transitions are intense, and they are unresolved within the intense low-energy feature.

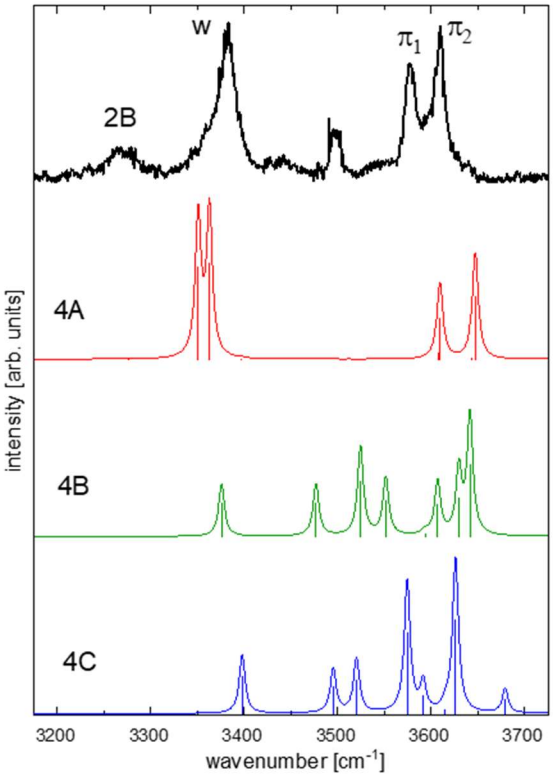

Figure 8. Infrared photodissociation spectrum of $Py^{-}\cdot(H_2O)_4\cdot Ar_2$ (top trace) in comparison with calculated IR spectra of the three lowest energy conformers (conformer label given for each curve, see Figure 9). The vertical sticks denote calculated frequency positions and intensities, the full lines show simulated spectra with 8 cm^{-1} full width at half-maximum (FWHM).

The high-energy modes of the conformer 4A are contained two peaks, each of which consists of a pair of unresolved transitions, one of which is strong, while the other is weak. The strongest transition, which is responsible for the peak at 3609 cm^{-1} (labeled π_2) involves the all-in-phase

linear combination of the OH oscillators forming π-H-bonds, while the peak at 3577 cm^{-1} (labeled π_1) is due to a mode where the two OH groups over the central rings of the Py^- frame oscillate in phase with a large amplitude, while the two OH groups over the outer rings both oscillate with a smaller amplitude and the opposite phase. Both of the higher energy features are due to linear combinations of the antisymmetric stretching vibrations of the water molecules.

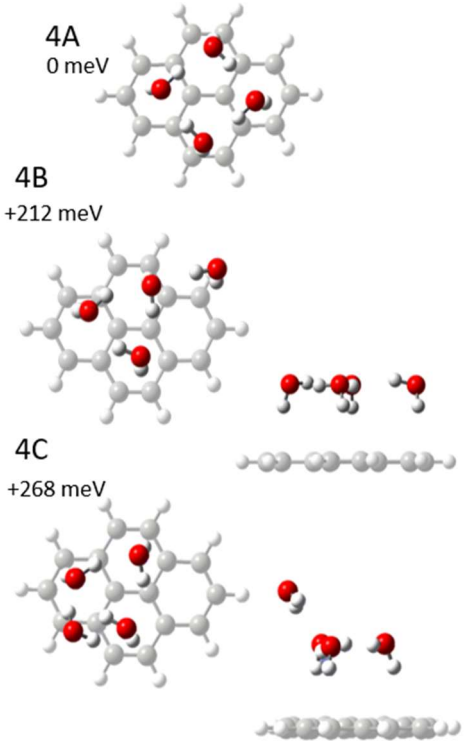

Figure 9. Low-lying minimum energy structures of $Py^-\cdot(H_2O)_4$, with relative energies given below each structure. The two structures shown in the center and bottom rows both belong to conformer 4B and 4C, respectively (left: top view, right: side view). Color scheme: C = grey, H = white, O = red. The Py^- frame has been de-emphasized to more clearly show the water positions.

We assign the broad feature around 3266 cm^{-1} (labeled 2B) to overtones and combination bands of the water bending modes. They are more intense than for the smaller clusters, since the symmetric OH stretching features for the tetrahydrate are lower in energy, increasing Fermi

resonance coupling with the bending mode levels (see Figure 1). The remaining features in the tetrahydrate spectrum are likely caused by higher energy conformers. We tentatively assign the broad features around 3442 cm^{-1} and 3547 cm^{-1} to the weaker features of conformer 4B, while the sharp peak at 3497 cm^{-1} is compatible with the intense feature predicted for conformer 4C in the same region of the spectrum.

Curiously, the linewidth of the narrowest resonance decreases monotonically with increasing cluster size, from ca. 24 cm^{-1} (n = 1) to ca. 10 cm^{-1} (n = 4). At first glance, this result is surprising, because a decrease of the linewidth concomitant with an increase in the vibrational density of states seems counterintuitive. The sharpening of the lines comes about as – reinforced by water-water hydrogen bonds – the water networks become more geometrically constrained as the number of water molecules in the cluster increases. Water molecules in these more rigid structures experience smaller OH frequency fluctuations, reducing spectral diffusion and the resulting line broadening.

B. CH Stretching Modes

Figure 10 shows a zoom into the CH-stretching region of the spectra. This region is strongly congested, since it not only contains the CH stretching fundamentals, but also Fermi resonances with overtones (v = 2) and combination bands of HCH bending modes, similar to the analogous bands for neutral Py.[58-61] We refrain from detailed assignments in this region, which will be discussed elsewhere.[62] The overall envelope of the CH-stretching bands is similar for all levels of hydration, and it is insensitive to the structural details of the water sub-cluster. The most intense peak at 3022 cm^{-1} is red-shifted compared to its position in neutral Py[58-61] at ca. 3050 cm^{-1}. There is a noticeable blueshift of all bands by ca. 3 cm^{-1} per water molecule. This blue shift is most likely caused by the polarization and partial localization of the excess charge induced by the presence of

the water molecules. While the excess charge is mostly localized in the π system, some of it also enters the σ* orbitals associated with the CH groups, weakening these bonds and slightly shifting the vibrational frequencies to the red. As the charge is pulled into the π system and the water subcluster (and therefore out of the σ* orbitals, see Figure 11) by the presence of the water molecules, the CH bonds re-strengthen, shifting the CH stretching modes to the blue. A similar effect has been observed for $Np^{-}\cdot(H_2O)_n$ cluster ions, where this effect is stronger, with blue shifts of up to 10 cm^{-1} per water molecule. The smaller blue shift in hydrated Py^{-} anion clusters is consistent with the overall lower charge density compared to Np^{-}.

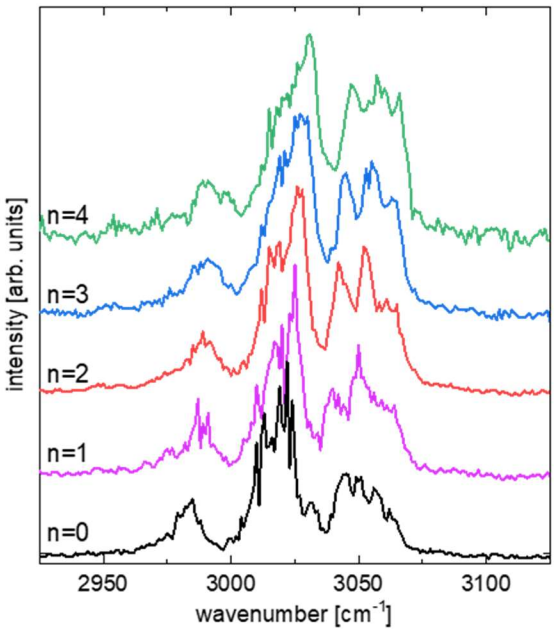

Figure 10. CH stretching region of the IR photodissociation spectra of $Py^{-}\cdot(H_2O)_n\cdot Ar_2$ ($n = 0 – 4$, indicated above each trace).

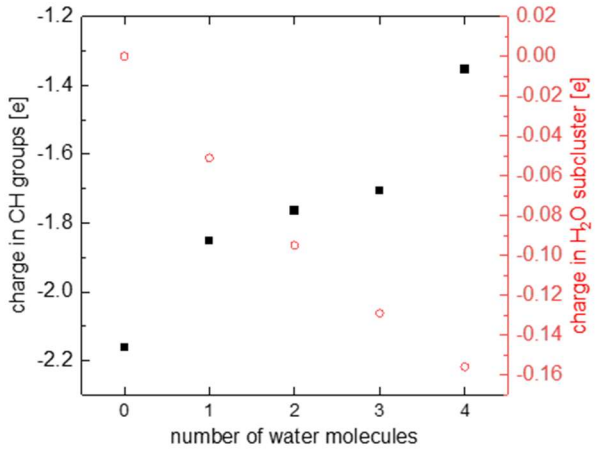

Figure 11. ESP charges on the CH groups (black squares, left axis) and on the water subcluster (red circles, right axis) as a function of the number of water molecules on $Py^{-}\cdot(H_2O)_n$.

IV. Conclusions

We have studied clusters of the form $Py^{-}\cdot(H_2O)_n\cdot Ar_2$ (n = 0 – 4) by infrared photodissociation spectroscopy. The OH stretching region is rich in infrared bands that encode the interaction of the water molecules with each other and with the π-system of the PAH anion. Water molecules condense into water networks on the PAH surface, whose water-water H-bonds are generally stronger than the H-bonds to the π system. At each cluster size, multiple conformers are populated. The relative energies of the lowest lying structures are very close for n = 1 and 2, while the minimum energy structures are well separated from higher energy geometries for n = 3 and 4, indicating that the higher lying conformers are populated during cluster growth and kinetically trapped. All OH groups are engaged in H-bonds with other water molecules or with the π system. Three- and four-membered rings form robust structural subunits for n = 3 and 4. The CH stretching region shows a weak blue shift of the very congested vibrational features with increasing cluster

size. This is consistent with a partial localization of the excess charge in the π-system by water molecules, which polarize the charge distribution and form H-bonds to the π-system.

ASSOCIATED CONTENT

Supporting Information. Mass spectrum of anionic pyrene and its hydrated clusters; experimental and calculated spectra of Py^- dihydrate; top and side view of $Py^-\cdot(H_2O)_2$ conformers; experimental and calculated spectra of Py^- trihydrate.; top and side view of $Py^-\cdot(H_2O)_3$ conformers; experimental and calculated spectra of Py^- tetrahydrate; top and side view of $Py^-\cdot(H_2O)_4$ conformers; patterns of motion of the symmetric OH stretching modes in conformer 4A; coordinates of selected conformers

The following files are available free of charge.

brief description (file type, i.e., PDF)

brief description (file type, i.e., PDF)

AUTHOR INFORMATION

Corresponding Author

*weberjm@jila.colorado.edu

ACKNOWLEDGMENT

We gratefully acknowledge support from the Department of Energy, Office of Basic Energy Sciences, under grant no. DE-SC0021387. This work utilized resources from the University of

Colorado Boulder Research Computing Group, which is supported by the National Science Foundation (awards ACI-1532235 and ACI-1532236), the University of Colorado Boulder, and Colorado State University.

REFERENCES

(1) Han, Y. M.; Bandowe, B. A. M.; Schneider, T.; Pongpiachan, S.; Ho, S. S. H.; Wei, C.; Wang, Q. Y.; Xing, L.; Wilcke, W. A 150-Year Record of Black Carbon (Soot and Char) and Polycyclic Aromatic Compounds Deposition in Lake Phayao, North Thailand. *Env. Pol.* **2021,** *269*, 116148.

(2) Li, X. R.; Zhao, Q.; Yang, Y.; Zhao, Z. Y.; Liu, Z. R.; Wen, T. X.; Hu, B.; Wang, Y. S.; Wang, L. L.; Wang, G. H. Composition and Sources of Brown Carbon Aerosols in Megacity Beijing During the Winter of 2016. *Atmos. Res.* **2021,** *262*, 105773.

(3) Wang, J. F.; Ye, J. H.; Zhang, Q.; Zhao, J.; Wu, Y. Z.; Li, J. Y.; Liu, D. T.; Li, W. J.; Zhang, Y. G.; Wu, C.; et al. Aqueous Production of Secondary Organic Aerosol from Fossil-Fuel Emissions in Winter Beijing Haze. *Proc. Natl. Acad. Sci. U. S. A.* **2021,** *118*, e2022179118.

(4) Mojiri, A.; Zhou, J. L.; Ohashi, A.; Ozaki, N.; Kindaichi, T. Comprehensive Review of Polycyclic Aromatic Hydrocarbons in Water Sources, Their Effects and Treatments. *Sci. Total Environ.* **2019,** *696*, 133971.

(5) Bourotte, C.; Forti, M. C.; Taniguchi, S.; Bicego, M. C.; Lotufo, P. A. A Wintertime Study of Pahs in Fine and Coarse Aerosols in Sao Paulo City, Brazil. *Atmos. Env.* **2005,** *39*, 3799-3811.

(6) Gogou, A.; Bouloubassi, I.; Stephanou, E. G. Marine Organic Geochemistry of the Eastern Mediterranean: 1. Aliphatic and Polyaromatic Hydrocarbons in Cretan Sea Surficial Sediments. *Marine Chem.* **2000,** *68*, 265-282.

(7) Yunker, M. B.; Macdonald, R. W.; Vingarzan, R.; Mitchell, R. H.; Goyette, D.; Sylvestre, S. Pahs in the Fraser River Basin: A Critical Appraisal of Pah Ratios as Indicators of PAH Source and Composition. *Org. Geochem.* **2002,** *33*, 489-515.

(8) Imanaka, H.; Khare, B. N.; Elsila, J. E.; Bakes, E. L. O.; McKay, C. P.; Cruikshank, D. P.; Sugita, S.; Matsui, T.; Zare, R. N. Laboratory Experiments of Titan Tholin Formed in Cold Plasma at Various Pressures: Implications for Nitrogen-Containing Polycyclic Aromatic Compounds in Titan Haze. *Icarus* **2004,** *168*, 344-366.

(9) Hardegree-Ullman, E. E.; Gudipati, M. S.; Boogert, A. C. A.; Lignell, H.; Allamandola, L. J.; Stapelfeldt, K. R.; Werner, M. Laboratory Determination of the Infrared Band Strengths of Pyrene Frozen in Water Ice: Implications for the Composition of Interstellar Ices. *Astrophys. J.* **2014,** *784*, 172.

(10) Quirico, E.; Moroz, L. V.; Schmitt, B.; Arnold, G.; Faure, M.; Beck, P.; Bonal, L.; Ciarniello, M.; Capaccioni, F.; Filacchione, G.; et al. Refractory and Semi-Volatile Organics at the Surface of Comet 67P/Churyumov-Gerasimenko: Insights from the Virtis/Rosetta Imaging Spectrometer. *Icarus* **2016,** *272*, 32-47.

(11) Derenne, S.; Robert, F. Model of Molecular Structure of the Insoluble Organic Matter Isolated from Murchison Meteorite. *Meteorit. Planet. Sci.* **2010,** *45*, 1461-1475.

(12) Jenniskens, P.; Baratta, G. A.; Kouchi, A.; Degroot, M. S.; Greenberg, J. M.; Strazzulla, G. Carbon Dust Formation on Interstellar Grains. *Astron. Astrophys.* **1993,** *273*, 583-600.

(13) Tielens, A. Interstellar Polycyclic Aromatic Hydrocarbon Molecules. *Annu. Rev. Astron. Astrophys.* **2008,** *46*, 289-337.

(14) Ostrowski, J. H. J.; Eaves, J. D. The Tunable Hydrophobic Effect on Electrically Doped Graphene. *J. Phys. Chem. B* **2014,** *118*, 530-536.

(15) Strong, S. E.; Eaves, J. D. Atomistic Hydrodynamics and the Dynamical Hydrophobic Effect in Porous Graphene. *J. Phys. Chem. Lett.* **2016,** *7*, 1907-1912.

(16) Rafiee, J.; Mi, X.; Gullapalli, H.; Thomas, A. V.; Yavari, F.; Shi, Y.; Ajayan, P. M.; Koratkar, N. A. Wetting Transparency of Graphene. *Nat. Mater.* **2012,** *11*, 217-222.

(17) Vernon, M. F.; Krajnovich, D. J.; Kwok, H. S.; Lisy, J. M.; Shen, Y. R.; Lee, Y. T. Infrared Vibrational Predissociation Spectroscopy of Water Clusters by the Crossed Laser-Molecular Beam Technique. *J. Chem. Phys.* **1982,** *77*, 47-57.

(18) Zwier, T. S. Laser Spectroscopy of Jet-Cooled Biomolecules and Their Water-Containing Clusters: Water Bridges and Molecular Conformation. *J. Phys. Chem. A* **2001,** *105*, 8827-8839.

(19) Robertson, W. H.; Johnson, M. A. Molecular Aspects of Halide Ion Hydration: The Cluster Approach. *Annu. Rev. Phys. Chem.* **2003,** *54*, 173-213.

(20) Headrick, J. M.; Diken, E. G.; Walters, R. S.; Hammer, N. I.; Christie, R. A.; Cui, J.; Myshakin, E. M.; Duncan, M. A.; Johnson, M. A.; Jordan, K. D. Spectral Signatures of Hydrated Proton Vibrations in Water Clusters. *Science* **2005,** *308*, 1765-1769.

(21) Kamariotis, A.; Boyarkin, O. V.; Mercier, S. R.; Beck, R. D.; Bush, M. F.; Williams, E. R.; Rizzo, T. R. Infrared Spectroscopy of Hydrated Amino Acids in the Gas Phase: Protonated and Lithiated Valine. *J. Am. Chem. Soc.* **2006,** *128*, 905-916.

(22) Asmis, K. R.; Neumark, D. M. Vibrational Spectroscopy of Microhydrated Conjugate Base Anions. *Acc. Chem. Res.* **2012,** *45*, 43-52.

(23) Nagornova, N. S.; Rizzo, T. R.; Boyarkin, O. V. Interplay of Intra- and Intermolecular H-Bonding in a Progressively Solvated Macrocyclic Peptide. *Science* **2012,** *336*, 320-323.

(24) Voss, J. M.; Fischer, K. C.; Garand, E. Accessing the Vibrational Signatures of Amino Acid Ions Embedded in Water Clusters. *J. Phys. Chem. Lett.* **2018,** *9*, 2246-2250.

(25) Xantheas, S. S. Cooperativity and Hydrogen Bonding Network in Water Clusters. *Chemical Physics* **2000,** *258*, 225-231.

(26) Myshakin, E. M.; Jordan, K. D.; Sibert, E. L.; Johnson, M. A. Large Anharmonic Effects in the Infrared Spectra of the Symmetrical $CH_3NO_2^{-}\cdot(H_2O)$ and $CH_3CO_2^{-}\cdot(H_2O)$ Complexes. *J. Chem. Phys.* **2003,** *119*, 10138-10145.

(27) Huang, X. C.; Braams, B. J.; Carter, S.; Bowman, J. M. Quantum Calculations of Vibrational Energies of $H_3O_2^{-}$ on an Ab Initio Potential. *J. Am. Chem. Soc.* **2004,** *126*, 5042-5043.

(28) McCoy, A. B.; Boyer, M. A. Exploring Expansions of the Potential and Dipole Surfaces Used for Vibrational Perturbation Theory. *J. Phys. Chem. A* **2022,** *126*, 7242-7249.

(29) Egan, C. K.; Paesani, F. Assessing Many-Body Effects of Water Self-Ions. I: $OH^{-}(H_2O)_n$ Clusters. *J. Chem. Theory Comput.* **2018,** *14*, 1982-1997.

(30) Paesani, F.; Yoo, S.; Bakker, H. J.; Xantheas, S. S. Nuclear Quantum Effects in the Reorientation of Water. *J. Phys. Chem. Lett.* **2010,** *1*, 2316-2321.

(31) Alata, I.; Broquier, M.; Dedonder-Lardeux, C.; Jouvet, C.; Kim, M.; Sohn, W. Y.; Kim, S. S.; Kang, H.; Schutz, M.; Patzer, A.; Dopfer, O. Microhydration Effects on the Electronic Spectra of Protonated Polycyclic Aromatic Hydrocarbons: Naphthalene-$(H_2O)_{n=1,2}H^{+}$. *J. Chem. Phys.* **2011,** *134*, 1-7.

(32) Attah, I. K.; Platt, S. P.; Meot-Ner, M.; El-Shall, M. S.; Aziz, S. G.; Alyoubi, A. O. Hydrogen Bonding of the Naphthalene Radical Cation to Water and Methanol and Attachment of the Naphthalene Ion to Extended Hydrogen Bonding Chains. *Chem. Phys. Lett.* **2014,** *613*, 45-53.

(33) Chatterjee, K.; Dopfer, O. Infrared Spectroscopy of Hydrated Polycyclic Aromatic Hydrocarbon Cations: Naphthalene^{+}-Water. *Phys. Chem. Chem. Phys.* **2017,** *19*, 32262-32271.

(34) Chatterjee, K.; Dopfer, O. Microhydration of PAH^{+} Cations: Evolution of Hydration Network in Naphthalene^{+}-$(H_2O)_n$ Clusters ($n \leq 5$). *Chem. Sci.* **2018,** *9*, 2301-2318.

(35) Guchhait, N.; Ebata, T.; Mikami, N. Vibrational Spectroscopy for Size-Selected Fluorene^{-}$(H_2O)_{n=1,2}$ Clusters in Supersonic Jets. *J. Phys. Chem. A* **2000,** *104*, 11891-11896.

(36) Chatterjee, K.; Roy, T. K.; Khatri, J.; Schwaab, G.; Havenith, M. Unravelling the Microhydration Frameworks of Prototype PAH by Infrared Spectroscopy: Naphthalene–$(Water)_{1–3}$. *Phys. Chem. Chem. Phys.* **2021,** *23*, 14016-14026.

(37) Loru, D.; Steber, A. L.; Pinacho, P.; Gruet, S.; Temelso, B.; Rijs, A. M.; Pérez, C.; Schnell, M. How Does the Composition of a PAH Influence Its Microsolvation? A Rotational Spectroscopy Study of the Phenanthrene–Water and Phenanthridine–Water Clusters. *Phys. Chem. Chem. Phys.* **2021,** *23*, 9721-9732.

(38) Loru, D.; Steber, A. L.; Pérez, C.; Obenchain, D. A.; Temelso, B.; López, J. C.; Schnell, M. Quantum Tunneling Facilitates Water Motion across the Surface of Phenanthrene. *J. Am. Chem. Soc.* **2023,** *145*, 17201-17210.

(39) Lemmens, A. K.; Ferrari, P.; Loru, D.; Batra, G.; Steber, A. L.; Redlich, B.; Schnell, M.; Martinez-Haya, B. Wetting of a Hydrophobic Surface: Far-Ir Action Spectroscopy and Dynamics of Microhydrated Naphthalene. *J. Phys. Chem. Lett.* **2023,** *14*, 10794-10802.

(40) Schiedt, J.; Knott, W. J.; Le Barbu, K.; Schlag, E. W.; Weinkauf, R. Microsolvation of Similar-Sized Aromatic Molecules: Photoelectron Spectroscopy of Bithiophene-, Azulene-, and Naphthalene-Water Anion Clusters. *J. Chem. Phys.* **2000,** *113*, 9470-9478.

(41) Lyapustina, S. A.; Xu, S. K.; Nilles, J. M.; Bowen, K. H. Solvent-Induced Stabilization of the Naphthalene Anion by Water Molecules: A Negative Cluster Ion Photoelectron Spectroscopic Study. *J. Chem. Phys.* **2000,** *112*, 6643-6648.

(42) Kawamata, H.; Maeyama, T.; Mikami, N. First Observation of Ionic Π-Hydrogen Bonds; Vibrational Spectroscopy of Dihydrated Naphthalene Anion ($Nph^-(H_2O)_2$). *Chem. Phys. Lett.* **2003,** *370*, 535-541.

(43) Knurr, B. J.; Adams, C. L.; Weber, J. M. Infrared Spectroscopy of Hydrated Naphthalene Cluster Anions. *J. Chem. Phys.* **2012,** *137*, 104303.

(44) Lietard, A.; Verlet, J. R. R. Effect of Microhydration on the Temporary Anion States of Pyrene. *J. Phys. Chem. Lett.* **2022,** *13*, 3529-3533.

(45) Schneider, H.; Vogelhuber, K. M.; Weber, J. M. Infrared Spectroscopy of Anionic Hydrated Fluorobenzene Complexes. *J. Chem. Phys.* **2007,** *127*, 114311.

(46) LeMessurier, N.; Salzmann, H.; Leversee, R.; Weber, J. M.; Eaves, J. D. Water-Hydrocarbon Interactions in Anionic Pyrene Monohydrate. *submitted* **2024**.

(47) Stoermer, C. W.; Gilb, S.; Friedrich, J.; Schooss, D.; Kappes, M. M. A High Resolution Dual Mass Gate for Ion Separation in Laser Desorption/Ionization Time of Flight Mass Spectrometry. *Rev. Sci. Instrum.* **1998,** *69*, 1661-1664.

(48) Wallace, W. E., Infrared Spectra. In *NIST Chemistry WebBook, NIST Standard Reference Database Number 69*, National Institute of Standards and Technology: Gaithersburg, MD.

(49) Parr, R. G.; Yang, W. *Density-Functional Theory of Atoms and Molecules*. Oxford University Press: New York, 1989.

(50) Chai, J. D.; Head-Gordon, M. Systematic Optimization of Long-Range Corrected Hybrid Density Functionals. *J. Chem. Phys.* **2008,** *128*.

(51) Weigend, F.; Ahlrichs, R. Balanced Basis Sets of Split Valence, Triple Zeta Valence and Quadruple Zeta Valence Quality for H to Rn: Design and Assessment of Accuracy. *Phys. Chem. Chem. Phys.* **2005,** *7*, 3297-3305.

(52) Frisch, M. J.; Trucks, G. W.; Schlegel, H. B.; Scuseria, G. E.; Robb, M. A.; Cheeseman, J. R.; Scalmani, G.; Barone, V.; Petersson, G. A.; Nakatsuji, H.; et al. *Gaussian 16 Rev. C.01*, Wallingford, CT, 2016.

(53) Singh, U. C.; Kollman, P. A. An Approach to Computing Electrostatic Charges for Molecules. *Journal of Computational Chemistry* **1984,** *5*, 129-145.

(54) Besler, B. H.; Merz Jr, K. M.; Kollman, P. A. Atomic Charges Derived from Semiempirical Methods. *J. Comput. Chem.* **1990,** *11*, 431-439.

(55) Klots, C. E. Evaporative Cooling. *J. Chem. Phys.* **1985,** *83*, 5854-5860.

(56) Ayotte, P.; Weddle, G. H.; Kim, J.; Johnson, M. A. Vibrational Spectroscopy of the Ionic Hydrogen Bond: Fermi Resonances and Ion-Molecule Stretching Frequencies in the Binary $X^-\cdot H_2O$ (X = Cl, Br, I) Complexes Via Argon Predissociation Spectroscopy. *J. Am. Chem. Soc.* **1998,** *120*, 12361-12362.

(57) Ayotte, P.; Weddle, G. H.; Johnson, M. A. An Infrared Study of the Competition between Hydrogen-Bond Networking and Ionic Solvation: Halide-Dependent Distortions of the Water Trimer in the $X^-\cdot(H_2O)_3$, (X = Cl, Br, I) Systems. *J. Chem. Phys.* **1999,** *110*, 7129-7132.

(58) Huneycutt, A. J.; Casaes, R. N.; McCall, B. J.; Chung, C. Y.; Lee, Y. P.; Saykally, R. J. Infrared Cavity Ringdown Spectroscopy of Jet-Cooled Polycylic Aromatic Hydrocarbons. *Chemphyschem* **2004,** *5*, 321-326.

(59) Mackie, C. J.; Candian, A.; Huang, X. C.; Maltseva, E.; Petrignani, A.; Oomens, J.; Mattioda, A. L.; Buma, W. J.; Lee, T. J.; Tielens, A. The Anharmonic Quartic Force Field Infrared Spectra of Five Non-Linear Polycyclic Aromatic Hydrocarbons: Benz a Anthracene, Chrysene, Phenanthrene, Pyrene, and Triphenylene. *J. Chem. Phys.* **2016,** *145*, 084313.

(60) Maltseva, E.; Petrignani, A.; Candian, A.; Mackie, C. J.; Huang, X. C.; Lee, T. J.; Tielens, A.; Oomens, J.; Buma, W. J. High-Resolution IR Absorption Spectroscopy of Polycyclic Aromatic Hydrocarbons in the 3 μm Region: Role of Periphery. *Astrophys. J.* **2016,** *831*.

(61) Mackie, C. J.; Candian, A.; Lee, T. J.; Tielens, A. G. G. M. Anharmonicity and the IR Emission Spectrum of Neutral Interstellar PAH Molecules. *J. Phys. Chem. A* **2022,** *126*, 3198-3209.

(62) Salzmann, H.; McCoy, A. B.; Weber, J. M. The Infrared Spectrum of Pyrene Anion in the Ch Stretching Region. *in preparation* **2024**.

TOC Graphic